# Passive Control of Self-Induced Roll Oscillations Using Bleed

T. Hu*, Z. Wang† and I. Gursul‡
*University of Bath, Bath, BA2 7AY, United Kingdom*

**A passive flow control method, which uses bleed from a slot near the wing tip, has been shown to attenuate self-excited roll oscillations of a low aspect ratio ($AR$ = 2) rectangular flat-plate wing. The effectiveness of the slot strongly depends on its location and width. For effective slot geometries, the tip vortex becomes more diffused, resulting in the elimination of the roll oscillations. Nonlinear interactions between the shear layers shed from the tip and the slot, as well as between the shear layer and the counter-rotating vortex may act as excitation, which can modify the response of the self-sustained oscillator. When the slot is located too close to the tip, there is rapid merging of the shear layers and less interactions, and the slot loses its effectiveness. Also, when the slot is narrow, there is insufficient bleed, resulting in less effective attenuation. Force measurements revealed that, this technique can be used as an effective method to suppress the roll oscillations without sacrificing the aerodynamic performance of the wing.**

## Nomenclature

| | | |
|---|---|---|
| $b$ | = | wing span |
| $c$ | = | wing root-chord length |
| $C_N$ | = | chord-normal force coefficient |
| $d$ | = | slot distance from tip |
| $D$ | = | drag force |
| $L$ | = | lift force |
| $N$ | = | normal force |
| $Re$ | = | Reynolds number, $\rho U_\infty c/\mu$ |
| $t$ | = | wing thickness |
| $U_{std}$ | = | standard deviation of velocity fluctuations |
| $U_\infty$ | = | freestream velocity |
| $\overline{U}$ | = | time-averaged velocity |
| $S$ | = | wing surface area |
| $S_L$ | = | effective area of lifting surface |
| $w$ | = | slot width |
| $x$ | = | chordwise coordinate |
| $\alpha$ | = | angle of attack |
| $\Gamma$ | = | circulation |
| $\mu$ | = | dynamic viscosity |
| $\rho$ | = | density |
| $\omega$ | = | instantaneous vorticity |
| $\overline{\omega}$ | = | time/phase-averaged vorticity |
| $\Phi$ | = | roll angle |
| $\Lambda$ | = | sweep angle |
| $AR$ | = | aspect ratio |
| FFT | = | fast Fourier transform |

* Postgraduate Student, Department of Mechanical Engineering.
† Lecturer, Department of Mechanical Engineering, Member AIAA.
‡ Professor, Department of Mechanical Engineering, Associate Fellow AIAA.

FTR = free-to-roll
LAR = low aspect ratio
MAV = micro air vehicle
PIV = particle image velocimetry
RMS = root-mean-square
UAV = unmanned air vehicle

## I. Introduction

Micro Air Vehicles[1] (MAVs) belong to a class of Unmanned Air Vehicles (UAVs) with a maximum dimension of less than 15 cm and a flight speed of about 10 $ms^{-1}$. MAVs are currently receiving growing interest because of their broad applications in commercial, research, military and other purposes. Various studies of low Reynolds number aerodynamics of low-aspect-ratio (LAR) wings have been conducted to improve the design of fixed wing MAVs[2,3]. However, in MAV flight tests[4], the onset of unwanted large-amplitude roll oscillations for various designs was reported, which eventually led to difficulties in flight control. Such flight instability was suggested[5] as an inherent issue due to the LAR wings and the low moment of inertia around its longitudinal axis.

Undesired roll oscillations, or "wing rock", were first studied for free-to-roll slender delta wings[6,7]. Wing rock is driven by the leading-edge vortex/wing interaction. Similar roll oscillations have also been reported in the studies of slender ($AR \leq 0.55$) rectangular wings[8,9]. Recent studies on free-to-roll non-slender delta wings[10,11] showed that self-induced roll oscillations also exist for delta wings with sweep angles $\Lambda \leq 60°$. More recently, further studies[12,13] were carried out for relatively higher aspect-ratio flat-plate wings ($AR$ = 2 and 4) with various planform shapes (rectangular, elliptical and Zimmerman). These studies showed that self-induced roll oscillations occurred prior to stall angle of attack and were initiated by the time-lag effects in the strength of tip vortices.

In order to suppress such undesired roll oscillations, a number of studies have been conducted using both active (oscillating flaps[14,15], blowing[16,17], acoustic excitation[18,19], and synthetic jets[20]) and passive[21-23] flow control techniques. The active control techniques included the use of acoustic excitation. In a recent study at the University of Bath, acoustic excitation was applied to attenuate the roll oscillations of an $AR$ = 2 rectangular flat plate wing[18,19]. It was found that the onset of the self-excited roll oscillations could be delayed by up to $\Delta\alpha_{max} \approx 4°$ and the magnitude of the oscillations was suppressed by up to $\Delta\Phi_{rms,max} \approx 30°$. More recently, a local excitation approach, in the form of a synthetic jet near the leading-edge of an $AR$ = 2 flat plate wing, was employed to supress the large amplitude oscillations, and significant reductions in the roll amplitude were observed[20].

Passive flow control strategies do not need external energy input therefore have advantages of simplicity and practicality. Early passive control techniques employed additional components/devices, such as divider fences[22], fins and winglets[21] and leading-edge devices[23]. Katz[7] reviewed these passive techniques and concluded that most of the passive techniques are limited and less effective in attenuation of wing rock. Moreover, previous studies of attenuation of wing rock suggested that passive flow control techniques using additional devices may result in adverse effects[21,23], such as extra drag and weight.

In this study we use bleed to control the wing rock. In contrast to active flow control methods such as blowing, bleed takes advantage of the pressure difference on the wing and is a passive flow control method that can be employed on demand. Bleed for two-dimensional airfoils has been investigated in detail to manipulate lift[24]. However, there is only one study for finite wings[25] and none for wing rock. Bleed through slots near the wing tip is generated by the pressure difference between the suction surface and the pressure surface of the wing. There is possibility that bleed may alter the location and structure of the wing tip vortex. The only study relevant to the tip vortices is the use of a partial slot near the wing tip, which is shown to diffuse the tip vortex[25]. The present study aims to demonstrate that the use of wing tip bleed can attenuate large amplitude roll oscillations of an $AR$ = 2 rectangular flat-plate wing.

## II. Experimental Apparatus and Methods

### A. Closed-loop wind tunnel

The experiments were conducted in a closed-loop wind tunnel at a constant freestream velocity of $U_\infty$ = 10 m/s ($Re = 1.14\times10^5$ based on wing chord length). The test section of the wind tunnel has dimensions of 2.13 × 1.52 × 2.70 m. The turbulence level of the wind tunnel is less than 0.1% of the freestream velocity. Figure 1 shows the experimental arrangement which includes the layout of the working section and the high-alpha rig. The wing models are attached to the high-alpha rig which allows the angle of attack to be varied as the wind tunnel is running with an accuracy of ±0.25 degrees.

### B. Free-to-roll (FTR) device

The free-to-roll device consists of a shaft that is supported in ultra-low-friction bearings which allow the shaft to rotate around its longitudinal axis with minimal friction. One end of the shaft is attached to a rotary variable transducer which outputs a varying voltage, linearly dependent on the roll angle, while the other end of the shaft is attached to the sting upon which the wing model is supported (Figure 1). The sting is mounted on the pressure surface of the wing model; the suction surface of the wing is flat. The output from the transducer is fed to the computer via an Analogue-Digital converter at a sampling frequency of 200 Hz for 120 seconds over a range of angles of attack with an estimated uncertainty of ±1º. From these data, the amplitude of the roll angle of the oscillations was calculated, as well as the maximum and minimum roll angles achieved during the recorded time period. Note that the sting used for all the models on the free-to-roll device were in line with the roll axis of the wings themselves, so there was no coning motion, just pure roll.

### C. Wing models

One baseline flat-plate wing of $AR = 2$ and six flat plate wing models with various wing tip slot width $w = 0.018c - 0.143c$ and slot locations of $d = 0.054c - 0.143c$ ($d$ is the distance between the wing tip and the slot centreline) were tested. The wings with various tip slots were named as tip slot A, B, C, D, E, F, respectively, as shown in Figure 2. The slots extended along the wing chord from 6 mm ($0.036c$) downstream of the leading-edge to 6 mm ($0.036c$) upstream of the wing trailing-edge. All the wing models have the same thickness ($t$ = 3 mm, 1.79% of chord length), span ($b$ = 335 mm) and chord length ($c$ =167.5 mm). Therefore, the effective aspect ratio of each wing is slightly different from that of the baseline model. The wing models were made out of aluminium plate with round edges (semi-circular shape). The maximum blockage was approximately 2.3%. The models were painted matt black in order to reduce reflections created from the laser sheet during the Particle Image Velocimetry (PIV) measurements.

### D. Particle Image Velocimetry (PIV) measurements

Velocity measurements at various crossflow planes ($x/c$ = 0.5, 0.75 and 1.05) were carried out using a TSI 2D particle image velocimetry (PIV) system. Illumination of the desired plane was achieved using dual 120 mJ Nd:YAG lasers. The laser sheets were placed perpendicular to the freestream (see Figure 1). The images were captured using a TSI PowerView Plus 12bit CCD camera with a resolution of 2048×2048 pixels from a downstream location shown in Figure 1. The camera was mounted on a camera support that is independent of the working section of the tunnel, so there is minimum vibration during the capturing. A TSI LaserPulse synchroniser unit was utilized to link the camera and the laser to enable accurate capture for the two frame cross-correlation analysis. The flow was seeded with olive oil droplets produced by a TSI model 9307-6 multi-jet atomizer. The mean size of the olive oil droplets was estimated as 1 μm. The system was operated at a sampling frequency of 7.25 Hz in the cross-correlation mode.

The PIV measurements were conducted for both stationary wings and free-to-roll wings with dynamic roll angle ($\Phi$) increasing and decreasing. For the stationary wing cases, the wing was clamped at the roll angle of $\Phi = 0º$. For the free-to-roll wing cases, phase-averaged velocity measurements were performed by triggering the PIV system at $\Phi = 0º$ during the roll oscillations. An error of ±0.5° in the trigger angle was estimated for these measurements. Sequences of 1000 instantaneous images were captured for each measurement. The images were analyzed using the software Insight 3G with a Fast Fourier Transform (FFT) cross-correlation algorithm and a Gaussian peak engine to obtain the velocity vectors. The recursive interrogation window size for time/phase averaged PIV measurements was 16 by 16 pixels and the effective grid size was 0.96 mm by 0.96 mm. The measurement uncertainty was estimated as 2% of the freestream velocity.

### E. Force measurements

The normal force coefficient was measured for the baseline model and modified wings with tip slots over a wing incidence range to study the effect of bleed on the wing aerodynamics. An ultra-low profile single component load cell (SMD S215) with maximum load capacity of 18 N was used for the force measurements. The load cell was integrated as a part of the sting upon which the wing was supported such that the force could be measured in the chord-normal direction, while the free-to-roll device was disabled and roll angle was fixed at $\Phi = 0º$. The output signal from the load cell was fed to a computer via an Analogue-Digital converter with a sampling frequency of 2 kHz and a time duration of 30 seconds for each measurement. The experimental uncertainty was estimated as 5%.

## III. Results and Discussion

### A. Self-excited roll oscillations

The time history of the wing roll angle was measured over a range of angles of attack (from 4º to 40º). Figure 3 presents the RMS values of the roll angle as a function of angle of attack for $AR$ = 2 flat-plate wing (baseline model). It can be observed that, similar to previous studies reported by Gresham *et al.*[12,13] and Hu *et al.*[18,19], the onset of self-excited roll oscillations is observed at around $\alpha$ = 12º for the baseline model. At 12º ≤ $\alpha$ < 15º, the roll amplitude gradually increases with increasing angle of attack. A sharp increase in roll amplitude is observed at 15º ≤ $\alpha$ < 22.5º. The stall angle of attack is $\alpha$ = 17º, hence large-amplitude roll oscillations begin just before the stall and continue in the post-stall region. Further increase in the wing incidence results in intermittent autorotation. At $\alpha$ = 27º, the autorotation stops and large amplitude roll oscillations occurs again. The amplitude of the roll oscillations however decreases sharply with further increase in the wing incidence. At $\alpha$ > 28°, the roll oscillations vanishes.

The variations of the RMS value of the roll angle as a function of angle of attack for flat plate wings with tip slots A to F are also plotted in Figure 3. For the largest wing tip slot A ($w$ = 0.143$c$), the self-excited roll oscillations are completely suppressed with only a small plateau of a few degrees observed in $\Phi_{rms}$ at 12º ≤ $\alpha$ ≤ 28º, corresponding to a maximum reduction of $\Delta\Phi_{rms,\,max} \approx$ 43º at $\alpha$ = 20º. Similar results are also obtained for flat plate wings with smaller tip slot widths of $w$ = 0.072$c$ (tip slots B and C) and $w$ = 0.036$c$ (tip slot D). The large amplitude roll oscillations are observed again at 16º ≤ $\alpha$ ≤ 24º for the wing with tip slot E, which has the same slot width as tip slot D but located closer to the wing tip. Its maximum amplitude is however smaller than that of the $AR$ = 2 flat plate wing. The present results suggest that the effectiveness of using bleed through relatively small slots to attenuate self-excited wing roll oscillations is very sensitive to its spanwise location (the wings with tip slots D and E have the same slot width but behave very differently). Similar large amplitude roll oscillations are also observed for the flat plate wing with the smallest slot width of $w$ = 0.018$c$ (tip slot F) at 15º ≤ $\alpha$ ≤ 28º with the maximum amplitude comparable to that of the $AR$ = 2 baseline model. Therefore, the results suggest that both the location and width of the slot affect the effectiveness of the bleed. Note that intermittent autorotation is not observed for wings with tip slot E and F (Figure 3).

### B. Velocity measurements

Previous studies suggest that the characteristics of the tip vortices that develop over rectangular wings play an important role in the onset and magnitude of the self-excited roll oscillations[13]. In order to understand the flow physics behind the variations of the RMS values of the roll angle as a function of angle of attack for various tip slots, phase-averaged and time-averaged PIV measurements were conducted in crossflow planes at chordwise locations of $x/c$ = 0.5, 0.75 and 1.05 over the baseline model and four wings with tip slots C, D, E and F, respectively, at $\alpha$ = 17º and $\Phi$ = 0º. In these experiments, both stationary and rolling wing cases were investigated. As expected, for the stationary baseline model, the time-averaged vorticity patterns near the left wing tip exhibit a coherent tip vortex. The tip vortex becomes larger with increasing streamwise distance in the downstream direction (Figure 4). Similar tip vortices are also observed from the phase-averaged vorticity patterns obtained by triggering the PIV system when the wing is rolling through $\Phi$ = 0º (Figure 4). Again, a coherent tip vortex is observed at all crossflow planes in the PIV measurements. However, the vortex is found further away from the wing surface when the wing is rolling in the counter-clockwise direction (increasing $\Phi$). In contrast, a coherent compact tip vortex is formed much closer to the wing surface when the wing is rolling in the clockwise direction (decreasing $\Phi$). Previous studies suggest that the asymmetric flows due to the hysteresis and time-lag effects of the tip vortices result in the self-induced roll oscillations[11-13].

Time-averaged and phase-averaged PIV measurements of crossflow vorticity patterns over the wing with tip slot C ($w$ = 0.072$c$) at chordwise locations of $x/c$ = 0.5, 0.75 and 1.05 for stationary wing, increasing $\Phi$, and decreasing $\Phi$, at $\Phi$ = 0º are presented in Figures 5 for $\alpha$ = 17º. As discussed in Section III-A, the large amplitude self-excited roll oscillations of the wing was completely suppressed by introducing tip slots A – D (Figure 3). Compared to tip slot A, tip slot C has a smaller slot width. In Figure 5, for the stationary wing, bleed through the slot is observed at various chordwise locations near the wing tip. The jet-like bleed results in the formation of a counter-rotating vortex, which is located close to and interacts with the shear layer separated from the wing tip. Furthermore, the clockwise vortex generated from the bleed develops into a larger vortical structure similar to the tip vortex over the baseline model. There appears to be an interaction between the regions of clockwise vorticity shed from the tip and the slot. As a result, the coherent tip vortex observed over the stationary baseline model (Figure 4) is not formed. Instead, only patches of vorticity, resembling the flow pattern over a slender body[26], are observed above the wing tip. Similar vorticity patterns are also obtained from the phase-averaged PIV measurements over the rolling wing with tip slot C at $\alpha$ = 17º and $\Phi$ = 0º for both increasing $\Phi$ and decreasing $\Phi$ cases. It is seen that the flow patterns of

the stationary wing and free-to-roll wing are similar, since the roll oscillations were nearly eliminated, and therefore no asymmetrical flow structure is observed. Modification to a coherent tip vortex due to the bleed results in a more diffused vortex, and attenuates the roll oscillations.

Figures 6 and 7 present time-averaged and phase-averaged crossflow vorticity patterns over the wings with tip slots of $w = 0.036c$ (but at different distances from the tip) at chordwise locations of $x/c = 0.5$, 0.75 and 1.05 for stationary wing, increasing $\Phi$, and decreasing $\Phi$, at $\Phi = 0^\circ$ and $\alpha = 17^\circ$. When the slot is located relatively further away from the wing tip (slot D), the vorticity patterns (Figure 6) are similar to those of tip slot C (Figure 5). For example, for the stationary wing, the counter-clockwise vortex generated by the bleed interacts with the shear layer separated from the wing tip. There is again an interaction between the regions of clockwise vorticity shed from the tip and the slot. These interactions prevent the formation of the coherent tip vortex observed over the stationary baseline model (Figure 4). Phase-averaged PIV measurements over the rolling wing with tip slot D do not reveal any hysteresis and time-lag effects, suggesting symmetric flow patterns which lead to the suppression of the roll oscillations (Figure 3).

Tip slot E has the same slot width of $w = 0.036c$ but is located closer to the wing tip. Time-averaged PIV measurements of crossflow vorticity patterns over the stationary wing with tip slot E shown in Figure 7 reveal that, for all chordwise locations of measurements, the shear layer separated from the wing tip merges with the clockwise vortex generated from the bleed through the tip slot, thus forming a coherent vortical structure similar to the coherent tip vortex observed over the $AR = 2$ baseline model. Phase-averaged PIV measurements of the crossflow vorticity patterns over the rolling wing with tip slot E at $\alpha = 17^\circ$ and $\Phi = 0^\circ$ indicate that the tip vortex is located further away from the wing surface for the increasing $\Phi$ case and closer to the wing surface for the decreasing $\Phi$ case (Figure 7). These hysteresis and time-lag effects are similar to those observed over the free-to-roll baseline model[12,13,18,19], suggesting the presence of the asymmetric flows which lead to the large amplitude self-induced roll oscillations again at $16^\circ \le \alpha \le 24^\circ$ (Figure 3).

For the wing with the smallest slot width of $w = 0.018c$ (tip slot F, for which the location of the center of the slot is the same as tip slot C), Figure 8 shows that coherent tip vortices over both stationary and free-to-roll wings, and the hysteresis for rolling wings are essentially the same as those of the $AR = 2$ baseline model. As the bleed flow is not strong, it does not interact with the tip vortex. The counter-rotating vortex generated by the bleed loiters near the tip slot and its interaction (if any) with the shear layer separated from the wing tip is not strong enough. As a result, large amplitude roll oscillations are observed again at $15^\circ \le \alpha \le 28^\circ$ with the maximum amplitude comparable to that of the $AR = 2$ baseline model (Figure 3). The present results suggest that the effectiveness of bleed through relatively small slot widths is sensitive to its spanwise location due to the relatively small momentum of the jet-like bleed.

Circulation of both clockwise and counter-clockwise vortices in the crossflow planes over the stationary $AR = 2$ baseline wing and four other wings with tip slots C, D, E and F at chordwise locations of $x/c = 0.5$, 0.75 and 1.05, $\alpha = 17^\circ$ and $\Phi = 0^\circ$ were calculated from the aforementioned time-averaged vorticity data. In this paper, the circulation was calculated using the area integration method, i.e., $\Gamma = \iint_S \bar{\omega}\, dS$, where $S$ is the area of the crossflow plane and $\bar{\omega}$ is the time-averaged vorticity shown in Figures 4-8. The variation of the absolute value of the normalized circulation, $|\Gamma|/U_\infty c$, as a function of the chordwise locations of the measurement planes is plotted in Figure 9. It can be seen that, for the $AR = 2$ baseline wing, the normalized circulation of clockwise vortices increases with $x/c$, while the circulation of counter-clockwise vorticity remains near zero, consistent with the PIV results that only the clockwise coherent tip vortex is generated over the stationary baseline model and the vortex is becoming stronger while evolving downstream (Figure 4). The variation of the absolute value of the normalized circulation for the modified wings with tip slots C – F exhibits similar trends to those of the baseline model, i.e., $|\Gamma|/U_\infty c$ of the clockwise vortices increase with $x/c$ and the absolute value of the normalized circulation of the counter-clockwise vortices remain relatively constant at $|\Gamma|/U_\infty c \approx 0.07$. Note that all the modified wings have comparable magnitude of the circulation. Furthermore, at each $x/c$, the absolute value of the circulation of the clockwise vortices is larger than that of the baseline model by about $\Delta|\Gamma|/U_\infty c \approx 0.07$, comparable to the circulation of the counter-clockwise vortices. This observation suggests that the total net circulation is not affected much by the bleed.

Figure 9 indicates that the wings with tip slots C – F exhibit comparable magnitudes of circulation for both clockwise and counter-clockwise vortices. Their effectiveness in attenuating large amplitude self-excited roll oscillations however varies substantially. For example, with tip slot C and D, the roll oscillations were completely suppressed; while the large amplitude roll oscillations were observed again for wings with tip slots E and F (Figure 3). In order to understand the differences better, close-up views of the flow near the slots were examined. Figures 10 and 11 show the time-averaged velocity magnitude and streamline patterns in the crossflow planes at chordwise locations of $x/c = 0.5$, 0.75 and 1.05 over stationary $AR = 2$ baseline wing and modified wings with tip slots C – F at

$\alpha$ = 17º and $\Phi$ = 0º. For the baseline wing, tightly closed streamlines corresponding to the location of the tip vortex are apparent. In contrast, for tip slots C and D, the closed streamline patterns indicate weaker (more diffused) vortices. This may be due to the interaction between the regions of vorticity shed from the tip and the slot. It is also noted that the crossflow velocity in the shear layer separated from the tip is smaller when there is a slot, which may be due to the decreasing pressure difference in the presence of a slot. Due to the bleed, jet-like high velocity regions are observed over the slots for the modified wings. For the wing with tip slot C, the bleed generates a counter-rotating vortex pair, which moves the low velocity region inboard compared to the $AR$ = 2 baseline model (Figure 10). The counter-clockwise vortex, however, stays close to the shear layer separated from the wing tip and produces a region of high velocity and reattachment near the wing tip. The reattachment region near the wing tip is highly unsteady as suggested by the large standard deviation of velocity fluctuations shown in Figure 12. Similar observations can also be made about the wing with tip slot D, i.e., high velocity due to the bleed, reattachment near the wing tip (Figure 10) and intensified unsteadiness as evidenced by large standard deviation of velocity fluctuations (Figure 12). It is also noted that, for the wing with tip slot D, the apparent center of the closed streamlines is more outboard. This may be due to the narrower slot located further away from the tip. Nevertheless, both tip slots C and D are effective in attenuating the roll oscillations.

Figure 11 shows that, for tip slots E and F, there are tightly closed streamlines similar to the baseline wing. The crossflow velocity in the shear layer separated from the tip appears to increase compared to the slots C and D. Tip slot E has the same slot width as tip slot D, $w = 0.036c$, but is located closer to the wing tip, which may affect the formation of the counter-rotating vortex. As the tip slot E is not as good as the tip slot D in attenuating the roll oscillations, there seems to be a lower limit of distance from the tip for effective slot geometry. Although the opposite (very large distance from the tip) has not been tested, it is likely that there will be an optimal distance of the slot from the tip.

It is observed from Figure 11 that, over the wing with tip slot E, the high velocity and reattachment regions are much smaller than that over the wing with tip slot D (Figure 10). Figure 13 shows smaller amplitude and smaller area of significant standard deviation of velocity fluctuations. This may indicate weaker interaction between the vortical regions separated from the wing tip and the slot. As a result, the coherent tip vortex is re-established from the separated shear layer and large amplitude roll oscillations are observed. For tip slot F, similar low level of unsteadiness due to the weak interaction between the vortices is also observed. Figures 12 and 13 show that the standard deviation of velocity fluctuations near the wing tip with tip slot F is significantly lower than those with tip slots C, D and E. Consequently, the tip vortex, which is of similar characteristics to those observed over the $AR$ = 2 baseline model, is formed and large roll oscillations are observed.

The present results suggest that the location and width of the slot affect the amount of the bleed and its interaction with the tip vortex as well as the strength of the shear layer separated from the tip. These factors may determine whether a strong interaction between the vortices take place and result in a diffused vortex, which leads to the attenuation of the roll oscillations. Figure 14 shows typical instantaneous crossflow vorticity patterns over the stationary $AR$ = 2 baseline model and modified wings with tip slot C - F at chordwise location of $x/c$ = 0.75, $\alpha$ = 17º and $\Phi$ = 0º. It is observed that, for the baseline model, the shear layer from the wing tip is rolling up into a coherent vortical structure. For the tip slots C and D, the shear layer vortices shed from the tip interact with the shear layer vortices shed from the slot. The increased unsteadiness of the flow for tip slots C and D is an indication of these vortical interactions. Similarly, it is suggested that nonlinear interactions between the vortices cause increased meandering of the leading-edge vortices[27] and the tip vortices[28]. Presumably, the interaction of the vortices will depend on the location of and width of the slot. When the slot is located close to the tip, the shear layers merge (tip slot E), and when the slot is narrow insufficient bleed does not generate strong enough interaction (tip slot F).

It is also noted that, in the cases where the roll oscillations were suppressed, there was strong unsteadiness between the shear layer separated from the tip and the counter-rotating vortex. There may be consequences of this on the development of the shear layer instabilities. In particular, for tip slot C, there is evidence of such interactions in the form of vortex pairs of opposite sign. Similarly, it is shown that the shear layer instabilities are affected by the secondary vortices of opposite sign over delta wings[29]. Also, it is expected that the shear layer will be highly susceptible to excitation near the wing tip[30].

Another aspect is that the unsteadiness between the tip shear layer and the bleed flow (especially counter-rotating vortex) may be considered as an external excitation to the self-excited roll oscillations resulting from the fluid-structure interaction. Excitation can modify the behaviour of a self-sustained oscillator substantially, and can even eliminate the oscillations. In a recent study[31], both increased and decreased roll oscillations are shown to be possible when forced pitch oscillations are imposed on a free-to-roll wing.

It is also noted that these suggested mechanisms differ from that for the active control of the wing rock of the same low aspect ratio wing[18-20]. In these studies, it has been shown that the excitation of the flow results in the

formation of the separated shear layer and tip vortices closer to the wing surface, which is more typical of lower wing incidence, thus effectively suppressing roll oscillations.

### C. Force measurements

PIV The present study indicates that the passive flow control technique using bleed through tip slots can be used to attenuate the large amplitude self-induced roll oscillations. This is best achieved when the tip vortex becomes diffused as a result of the bleed. However, previous studies also suggest that tip vortex plays an important role in the aerodynamics of the low aspect ratio (LAR) wings[3-5]. Therefore, it is interesting to explore to which extent the bleed through tip slots will affect the aerodynamic performance of the flat plate wings.

Figure 15 presents the variation of the normal force coefficient $C_N$ ($= \frac{N}{\frac{1}{2}\rho U_\infty^2 S_L}$) as a function of angle of attack of the $AR = 2$ baseline model and flat plate wings with tip slots A – F. Here $N$ is the normal force and $S_L$ is the effective lifting surface area (excluding the area of the slots) of the wings and $U_\infty$ is the freestream velocity. It can be observed that, for the $AR = 2$ baseline model, $C_N$ increases with wing incidence and reaches the maximum value of $C_{N,max} \approx 0.82$ at $\alpha = 17^\circ$. These results are in good agreement with the normal force coefficients of an $AR = 2$ flat plate rectangular wing reported by Torres and Mueller[3]. In this paper, the normal force $N$ of Torres and Mueller wing was calculated from their lift and drag data, i.e., $N = L \cos\alpha + D \sin\alpha$, where $L$ is the lift force, $D$ is the drag force and $\alpha$ is the angle of attack. Note that, at $\alpha \geq 13^\circ$, Torres and Mueller's results showed a slightly smaller $C_N$, and also $C_{N,max}$ at a larger angle of attack of $\alpha = 19^\circ$. This could be attributed to the slight differences in the Reynolds number, wing thickness and leading-edge profile. Figure 15 shows that, prior to $\alpha = 12^\circ$, $C_N$ of the flat plate wing with tip slot A is comparable to those of the baseline model. At $\alpha > 12^\circ$, the wing with tip slot A exhibits a larger $C_{N,max}$ of 0.97 at the angle of attack of 18º. In contrast, it was found that, $C_N$ of the wings with tip slots B and D were smaller than those of the baseline model by up to 12%. On the other hand, over the whole range of $\alpha$ tested, $C_N$ of the flat plate wings with tip slots C, E and F exhibit the same trends/magnitudes as those of the baseline model. In summary, the effect of the slots is negligible in the pre-stall region, while there is some effect on the stall angle and the maximum normal force coefficient for some of the wings.

.

## IV. Conclusions

A passive flow control technique that uses bleed through slots near the wing tip was employed to attenuate the self-excited roll oscillations of an $AR = 2$ free-to-roll rectangular flat plate wing. The time history of the wing roll angle was measured over a range of angles of attack in a wind tunnel. It was found that the $AR = 2$ baseline wing exhibited large amplitude roll oscillations that began before the stall angle. For appropriate tip slots, these roll oscillations can be suppressed completely for all angles of attack. The effectiveness was found to depend on the width and spanwise location of the slot.

Velocity measurements conducted over the wings showed that the jet-like bleed through tip slots resulted in the formation of a counter-rotating vortex, which may interact with the shear layer separated from the tip. Depending on the slot location and width, the presence of a slot may affect the magnitude of the cross-flow velocity in the shear layer shed from the tip. In the cases where the roll oscillations were suppressed, there is evidence that clockwise vorticity shed from the tip and the slot interact with each other. In these cases, the overall unsteadiness of the flow was larger, and the mean flow appeared as highly diffused with scattered vorticity concentrations. When the slot was close to the tip, clockwise vorticity shed from the tip and the slot merged without significant interaction, which resulted in a coherent vortex and large amplitude roll oscillations. When the slot was narrow, there was insufficient bleed and insufficient vortical interactions.

For the effective slot geometries, the flow field is highly unsteady, which may be due to the nonlinear interactions between the vortices. It is also noted that the unsteadiness of the counter-rotating vortex may affect the development of the shear layer shed from the tip. This may also serve as external excitation, which can modify the response of a self-sustained oscillator. These mechanisms differ from that for the active control techniques used for the same wing. The present force measurements suggested that, bleed through tip slots can be used as an effective approach to suppress the wing roll oscillations without sacrificing the aerodynamic performance of the wing. In contrast, it was found that the optimized tip slot arrangements could be used to delay stall and therefore obtain a larger maximum normal force coefficient.

## Acknowledgments

This work was supported by the RCUK Academic Fellowship in Unmanned Air Vehicles. The authors would like to thank the EPSRC Engineering Instrument Pool.

## References

[1]Shyy, W., Berg, M. and Ljungqvist, D., "Flapping and Flexible Wings for Biological and Microvehicles", *Progress in Aerospace Sciences*, Vol. 35, No. 5, 1999, pp. 455-506.

[2]Pelletier, A. and Mueller, T. J., "Low Reynolds Number Aerodynamics of Low-Aspect-Ratio, Thin/Flat/Cambered-Plate Wings", *Journal of Aircraft*, Vol. 37, No. 5, 2000, pp. 825- 832.

[3]Torres, G. E. and Mueller, T. J., "Low-Aspect-Ratio Wing Aerodynamics at Low Reynolds Numbers", *AIAA Journal*, Vol. 42, No. 5, 2004, pp. 865-873.

[4]Krashanitsa, R., Platanitis, G., Silin, D. and Shkarayev, S., "Autopilot Integration into Micro Air Vehicles", *Introduction to the Design of Fixed-Wing Micro Air Vehicles*, edited by Mueller, T., Kellogg, J., Ifju, P. and Shkarayev. S., AIAA, Reston, VA, 2007.

[5]Mueller, T., "An Overview of Micro Air Vehcile Aerodynamics", *Fixed and Flapping Wing Aerodynamics for Micro Air Vehicle Applications*, AIAA, Reston, VA, 2001.

[6]Arena, A. S. J. and Nelson, R. C., "Experimental Investigation on Limit Cycle Wing Rock of Slender Wings", *Journal of Aircraft*, Vol. 31, No. 5, 1994, pp. 1148-1155.

[7]Katz, J., "Wing/Vortex Interactions and Wing Rock", *Progress in Aerospace Sciences*, Vol. 35, No. 7, 1999, pp. 727-750.

[8]Levin, D. and Katz, J., "Self-Induced Roll Oscillations of Low-Aspect-Ratio Rectangular Wings", *Journal of Aircraft*, Vol. 29, No. 4, 1992, pp. 698-702.

[9]Williams, D. L. and Nelson, R. C., "Fluid-Dynamic Mechanisms Leading to the Self-Induced Oscillations of LARR wings", *35th Aerospace Sciences Meeting & Exhibit*, AIAA Paper 1997-0830, Jan 1997.

[10]Gursul, I., Gordnier, R. and Visbal, M., "Unsteady Aerodynamics of Nonslender Delta Wings", *Progress in Aerospace Sciences*, Vol. 41, No. 7, 2005, pp. 515-557.

[11]Gresham, N. T., Wang, Z. and Gursul, I., "Vortex Dynamics of Free-to-Roll Slender and Nonslender Delta Wings", *Journal of Aircraft*, Vol. 47, No. 1, 2010, pp. 292-302.

[12]Gresham, N. T., Wang, Z. and Gursul, I., "Self-Iinduced Roll Oscillation of Non-Slender Wings", *AIAA Journal*, Vol. 47, No. 3, 2009, pp. 481-483.

[13]Gresham, N. T., Wang, Z. and Gursul, I., "Low Reynolds Number Aerodynamics of Free-to-Roll Low Aspect Ratio Wings", *Experiments in Fluids*, Vol. 49, No.1, 2010, pp. 11-25.

[14]Walton, J. and Katz, J., "Reduction of Wing Rock Amplitudes Using Leading-Edge Vortex Manipulations", *30th Aerospace Sciences Meeting & Exhibit*, AIAA Paper 1992-0279, Jan 1992.

[15]Katz, J. and Walton, J., "Application of Leading-Edge Vortex Maniplations to Reduce Wing Rock Amplitudes", *Journal of Aircraft*, Vol. 30, No. 4, 1993, pp. 555-557.

[16]Wong, G. S., Rock, S. M., Wood, N. J. and Roberts, L., "Active Control of Wing Rock Using Tangential Leading-Edge Blowing", *Journal of Aircraft*, Vol. 31, No. 3, 1994, pp. 659-665.

[17]Sreenatha, A. G. and Ong, T. K., "Wing Rock Suppression Using Recessed angle Spanwise Blowing", *Journal of Aircraft*, Vol. 39, No. 5, 1994, pp. 900-903.

[18]Hu, T., Wang, Z. and Gursul, I., "Control of Self-Excited Roll Oscillations of Low-Aspect-Ratio Wings Using Acoustic Excitation", *49th AIAA Aerospace Sciences Meeting Including The New Horizons Forum and Aerospace Exposition*, AIAA Paper 2011-0036, Jan 2011.

[19]Hu, T., Wang, Z. and Gursul, I., "Attenuation of Self-Excited Roll Oscillation of Low-Aspect-Ratio Wings by Means of Acoustic Forcing", *AIAA Journal*, 2013, in print.

[20]Hu, T., Wang, Z. and Gursul, I., "Active Control of Self-Induced Roll Oscillations of a Wing Using Synthetic Jet", *International Journal of Flow Control*, 2013, under review.

[21]Synolakis C. E., Breuel B. D., Tegulapalle M. and Ho C. H., "Passive Control of delta Wing Rock", *Journal of Aircraft*, Vol. 30, No. 1, 1993, pp 131-135.

[22]Ng, T. T., Skaff, T. and Kountz, J., "Effect of Leeward Flow Dividers on the Wing Rock of a Delta Wing", *Journal of Aircraft*, Vol. 31, No. 6, 1994, pp. 1431-1433.

[23]Mabey, D. G., "Similitude Relations for Buffet and Wing Rock on Delta Wings", *Progress in Aerospace Sciences*, Vol. 33, No. 7-8, 1997, pp. 481-511.

[24]Kearney, J. M. and Glezer, A., "Aero-Effected Flight Control Using Distributed Active Bleed", *41st AIAA Fluid Dynamics Conference and Exhibit*, AIAA Paper 2011-3099, Jun 2011.

[25]Jin, J., Oh, S. and Yee, K., "Trailing Vortex Strength Attenuation via Chipped Wingtip Shapes", *31st AIAA Applied Aerodynamics Conference*, AIAA Paper 2013-2656, Jun 2013.

[26]Zeiger, M. D., Telionis D. P. and Vlachos P. P., "Unsteady Separated Flows over Three-Dimensional Slender Bodies", *Progress in Aerospace Sciences*, Vol. 40, No. 4-5, 2004, pp. 291-320.

[27]Gursul, I. and Xie, W., "Origin of Vortex Wandering over Delta Wings", *Journal of Aircraft*, Vol. 37, No. 2, 2000, pp. 348-350.

[28]Sen, R., "Vortex-Oscillation Model of Airfoil Side-Edge Noise", *AIAA Journal*, Vol. 35, No. 3, 1997, pp. 441-449.

[29]Visbal, M. R. and Gordnier, R. E., "Origin of Computed Unsteadiness in the Shear Layer of Delta Wings", *Journal of Aircraft*, Vol. 32, No. 5, 1995, pp. 1146-1148.
[30]Gordnier, R. E. and Visbal, M. R., "Unsteady Vortex Structure over a Delta Wing", *Journal of Aircraft*, Vol. 31, No. 1, 1994, pp. 243-248.
[31]Tregidgo, L., Wang, Z. and Gursul, I., "Frequency Lock-in Phenomenon for Self-Sustained Roll Oscillations of Rectangular Wings Undergoing a Forced Periodic Pitching Motion", *Physics of Fluids*, Vol. 24, No. 11, 2012, pp. (117101)1-18.

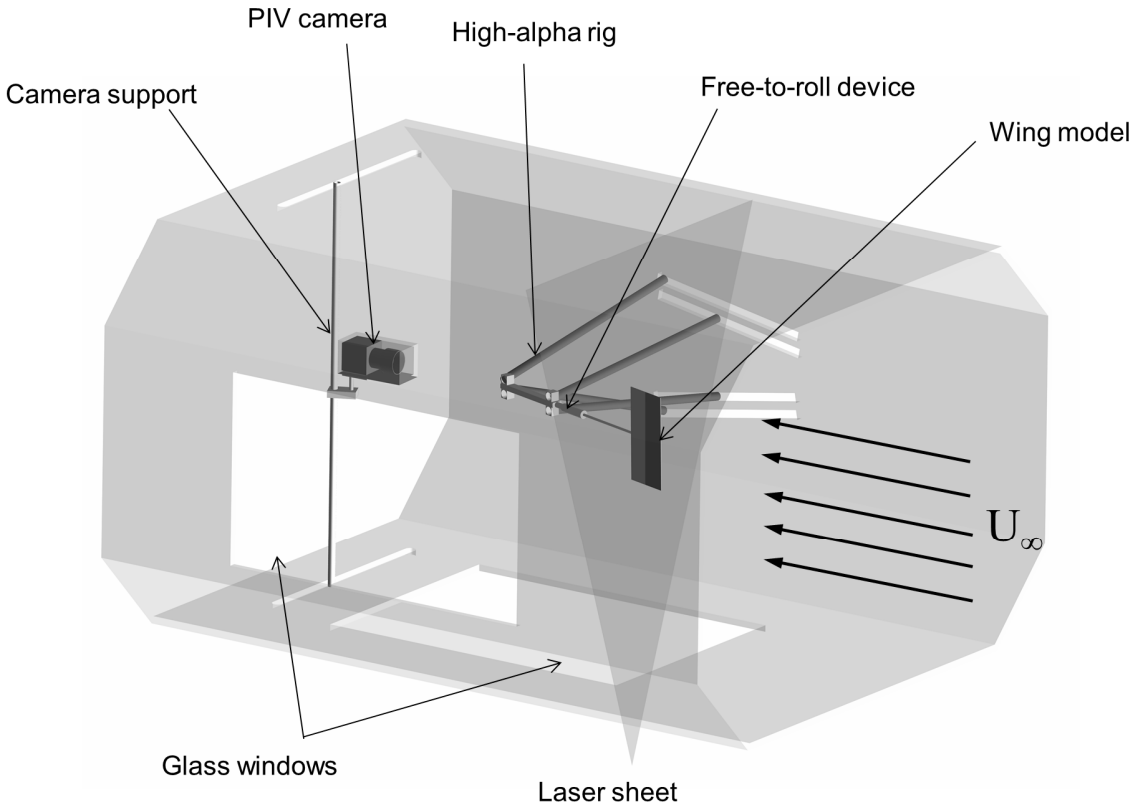


**Figure 1. Schematic of experimental setup.**

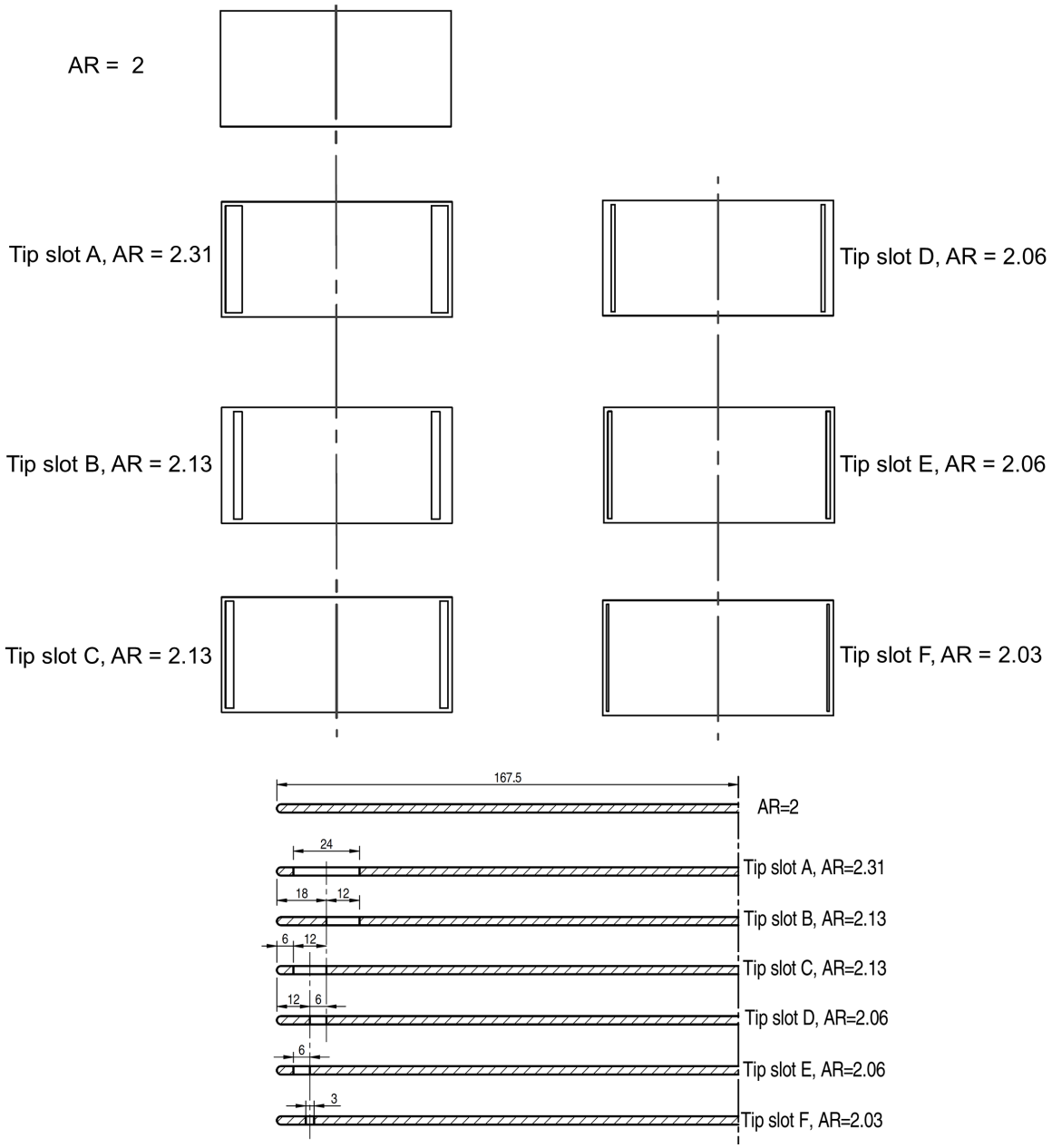


**Figure 2. Planform view of flat plate wings (top) and cross-sectional views (bottom) with dimensions (in mm) of the tip slots.**

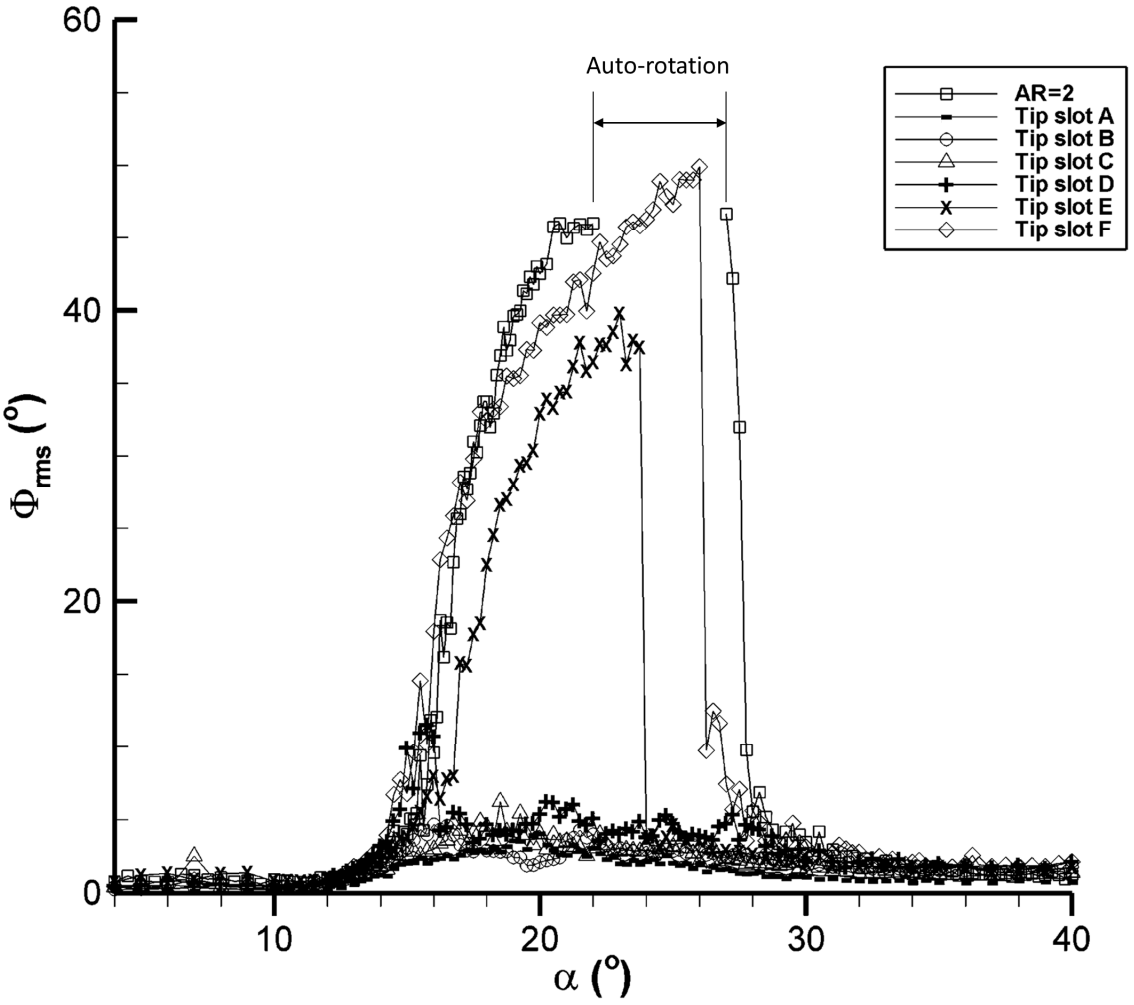


**Figure 3. RMS value of the wing roll angle as a function of angle of attack for *AR* = 2 baseline wing and flat plate wings with tip slots A to F.**

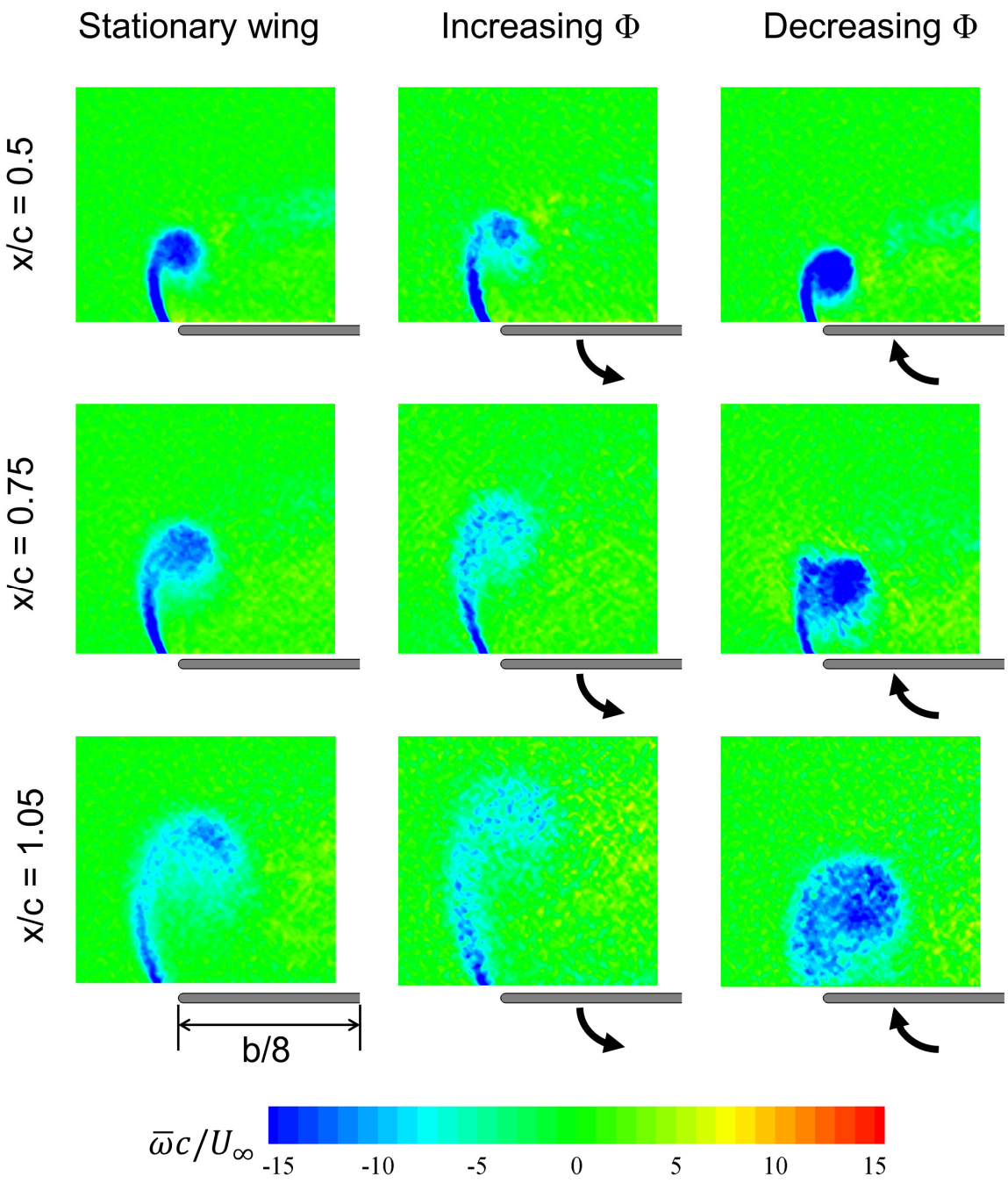


**Figure 4. Time and phase-averaged vorticity patterns over the *AR*=2 baseline wing at chordwise locations of *x/c* = 0.5, 0.75 and 1.05 for stationary wing, increasing *Φ*, and decreasing *Φ* at *Φ* = 0° and *α* = 17°.**

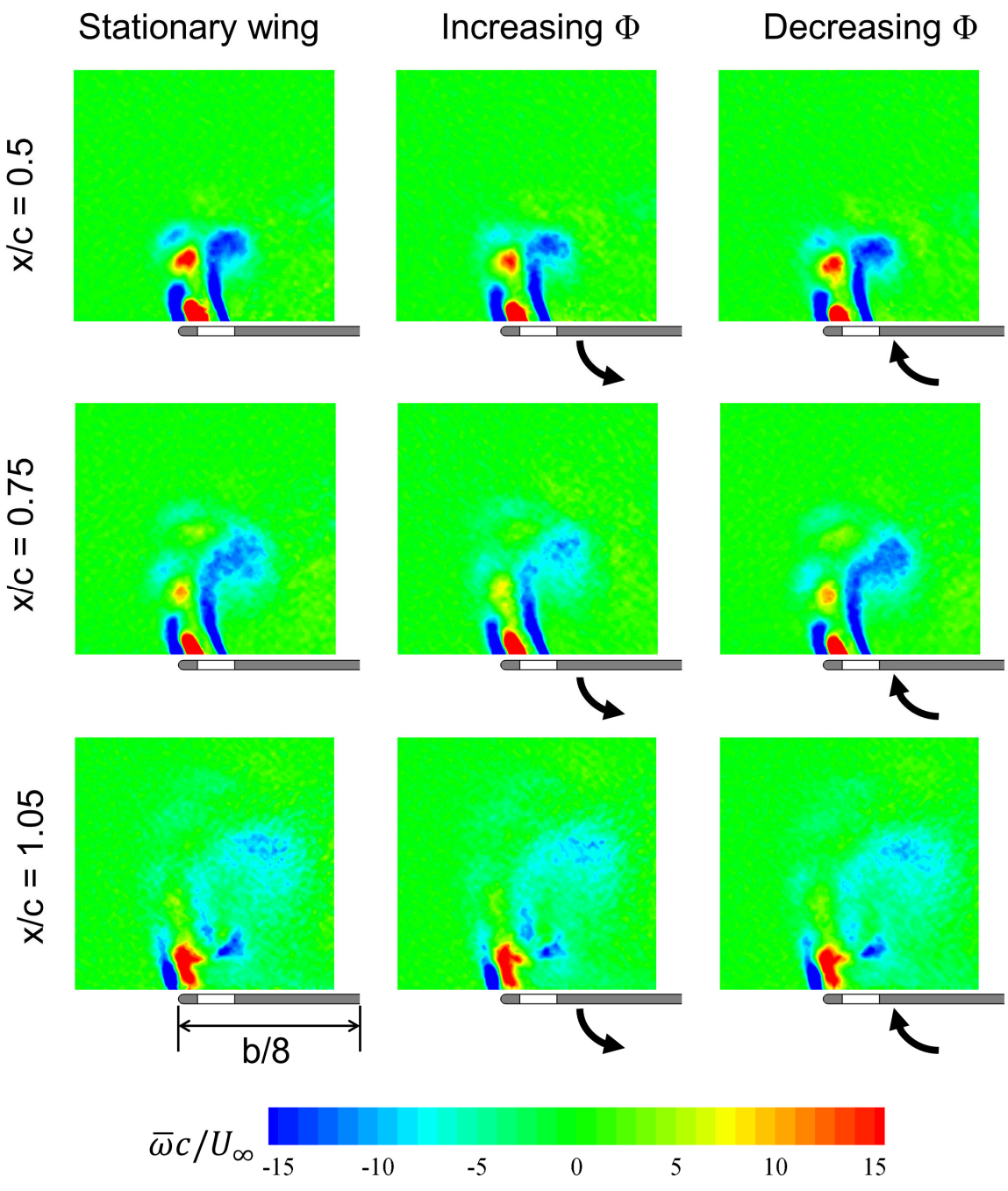


**Figure 5. Time and phase-averaged vorticity patterns over the wing with tip slot C at chordwise locations of *x/c* = 0.5, 0.75 and 1.05 for stationary wing, increasing *Φ*, and decreasing *Φ* at *Φ* = 0° and *α* = 17°.**

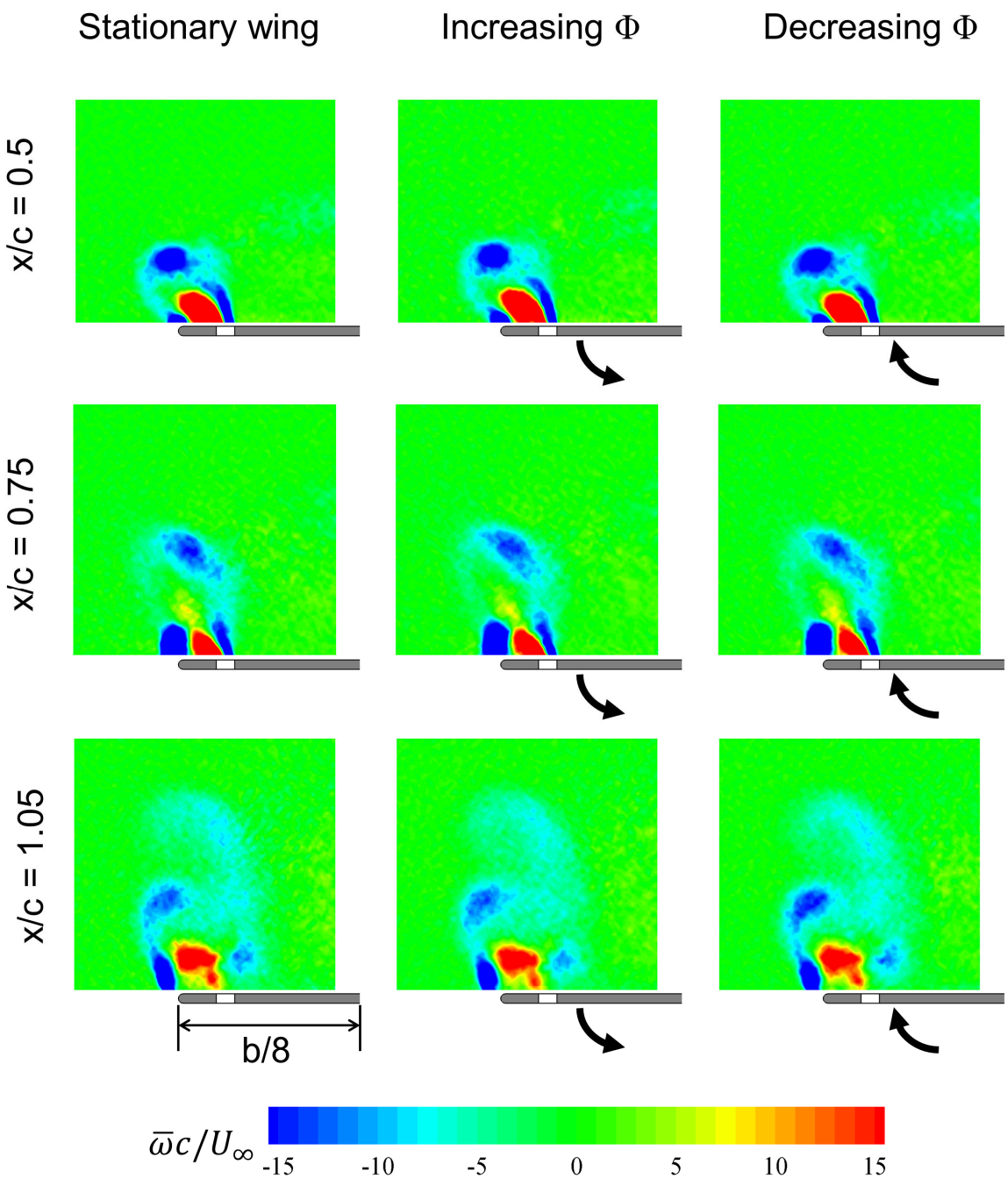


**Figure 6. Time and phase-averaged vorticity patterns over the wing with tip slot D at chordwise locations of *x/c* = 0.5, 0.75 and 1.05 for stationary wing, increasing *Φ*, and decreasing *Φ* at *Φ* = 0° and *α* = 17°.**

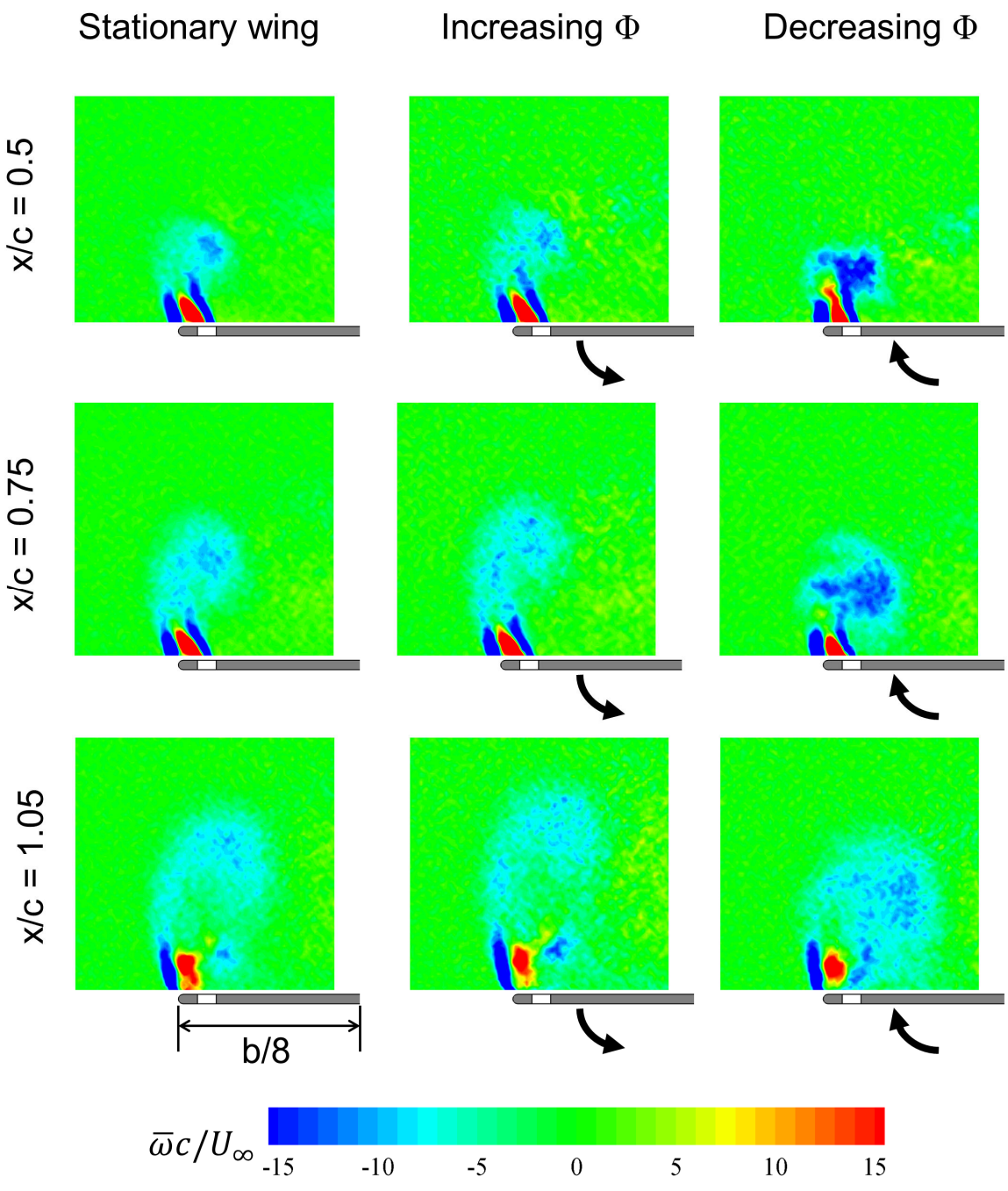


**Figure 7. Time and phase-averaged vorticity patterns over the wing with tip slot E at chordwise locations of $x/c$ = 0.5, 0.75 and 1.05 for stationary wing, increasing $\Phi$, and decreasing $\Phi$ at $\Phi$ = 0° and $\alpha$ = 17°.**

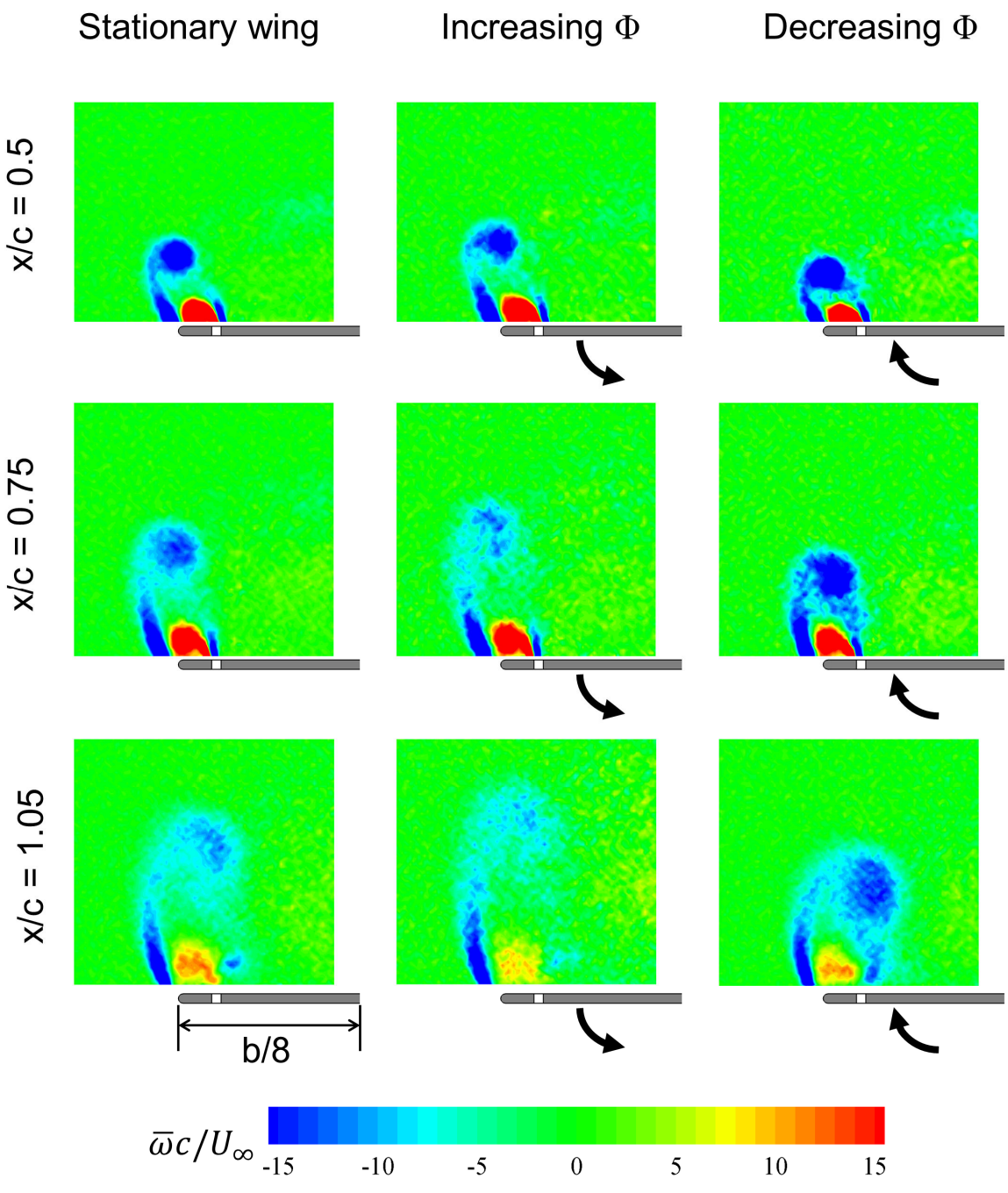


**Figure 8. Time and phased-averaged vorticity patterns over the wing with tip slot F at chordwise locations of *x/c* = 0.5, 0.75 and 1.05 for stationary wing, increasing *Φ* and decreasing *Φ* at *Φ* = 0° and *α* = 17°.**

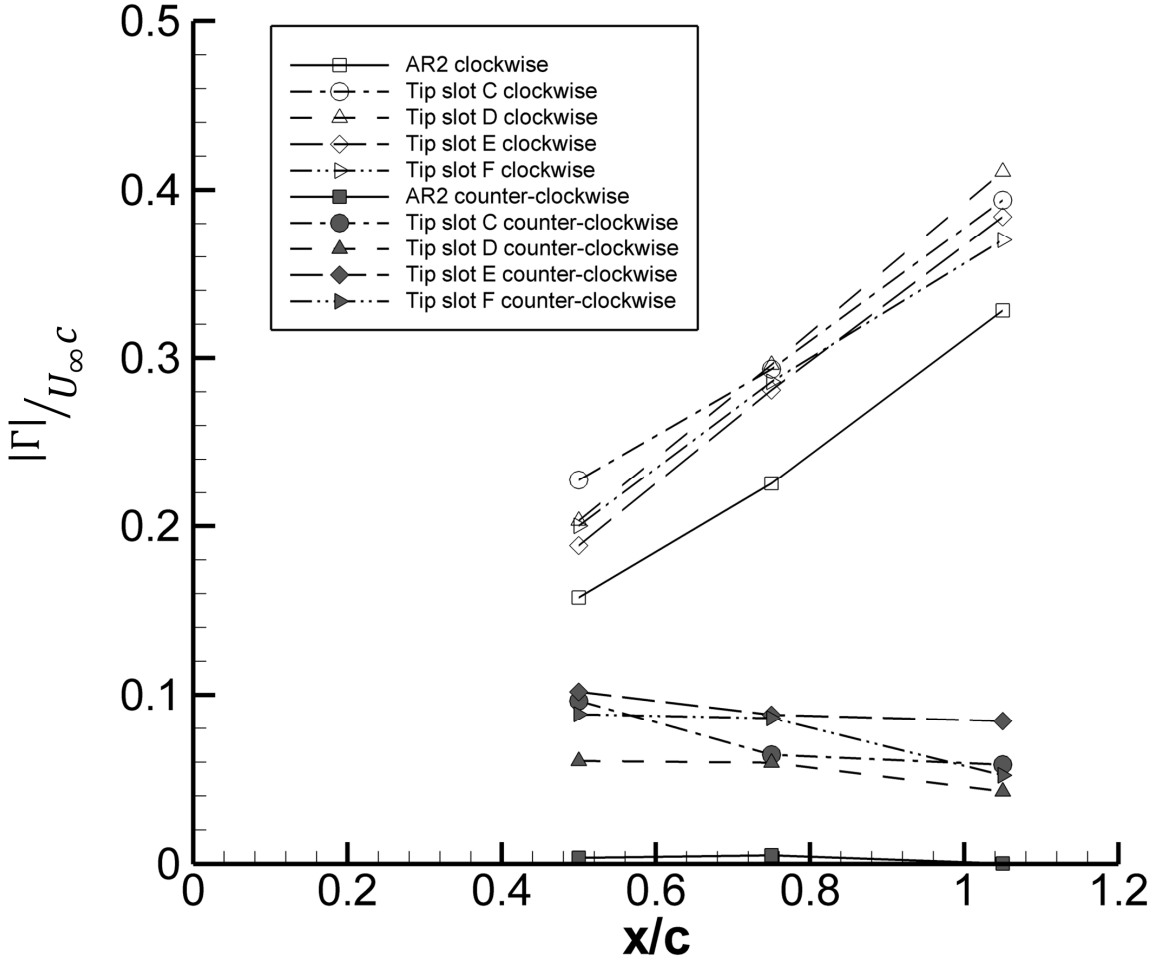


**Figure 9. Variation of absolute value of normalized circulation of the clockwise and counter-clockwise vortices over stationary wings at $\alpha$ = 17º and $\Phi$ = 0º.**

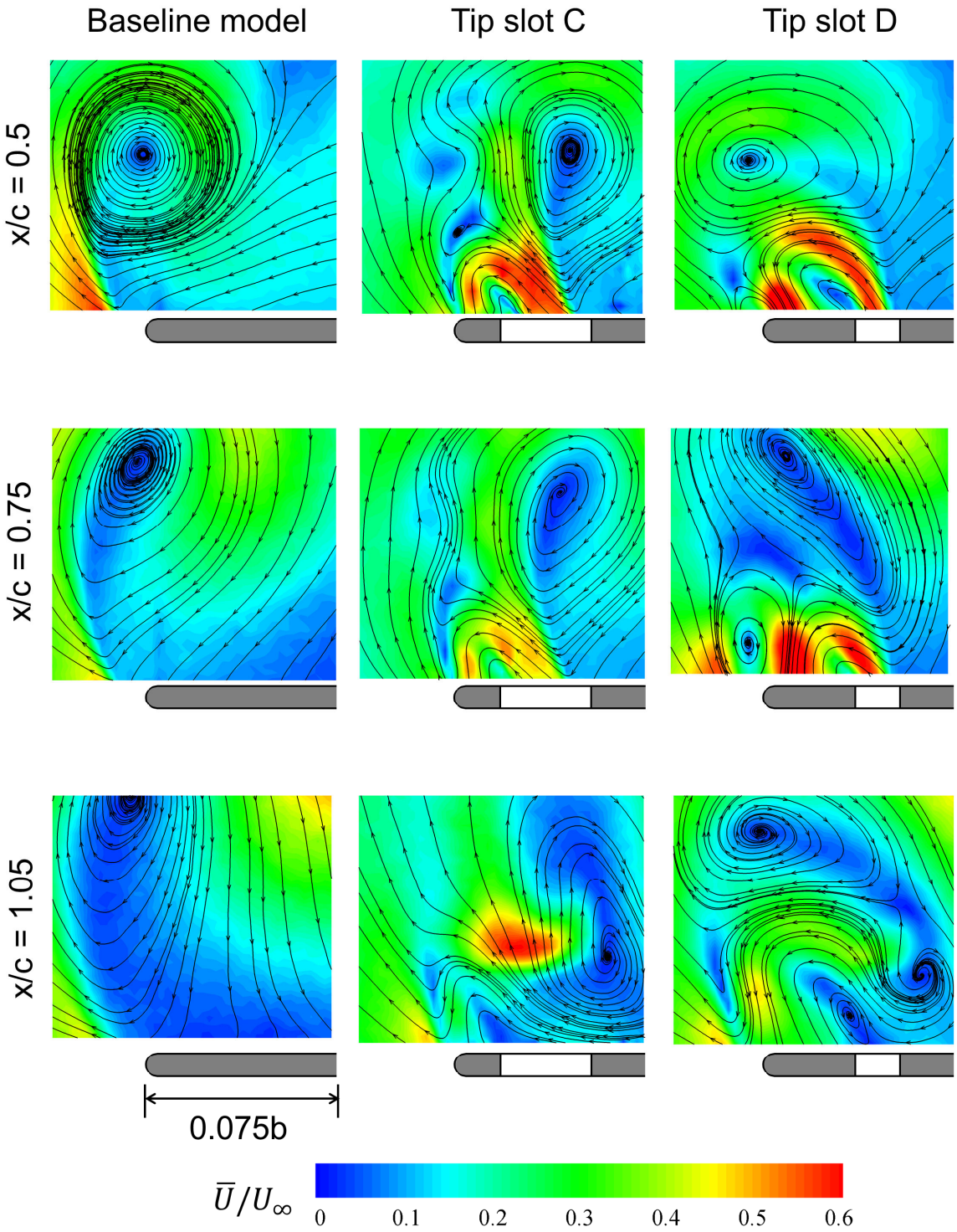


**Figure 10. Time-averaged velocity magnitude and streamline patterns over the stationary $AR$ = 2 baseline wing and flat plate wings with tip slot C and D at chordwise locations of $x/c$ = 0.5, 0.75 and 1.05 at $\alpha$ = 17° and $\Phi$ = 0°.**

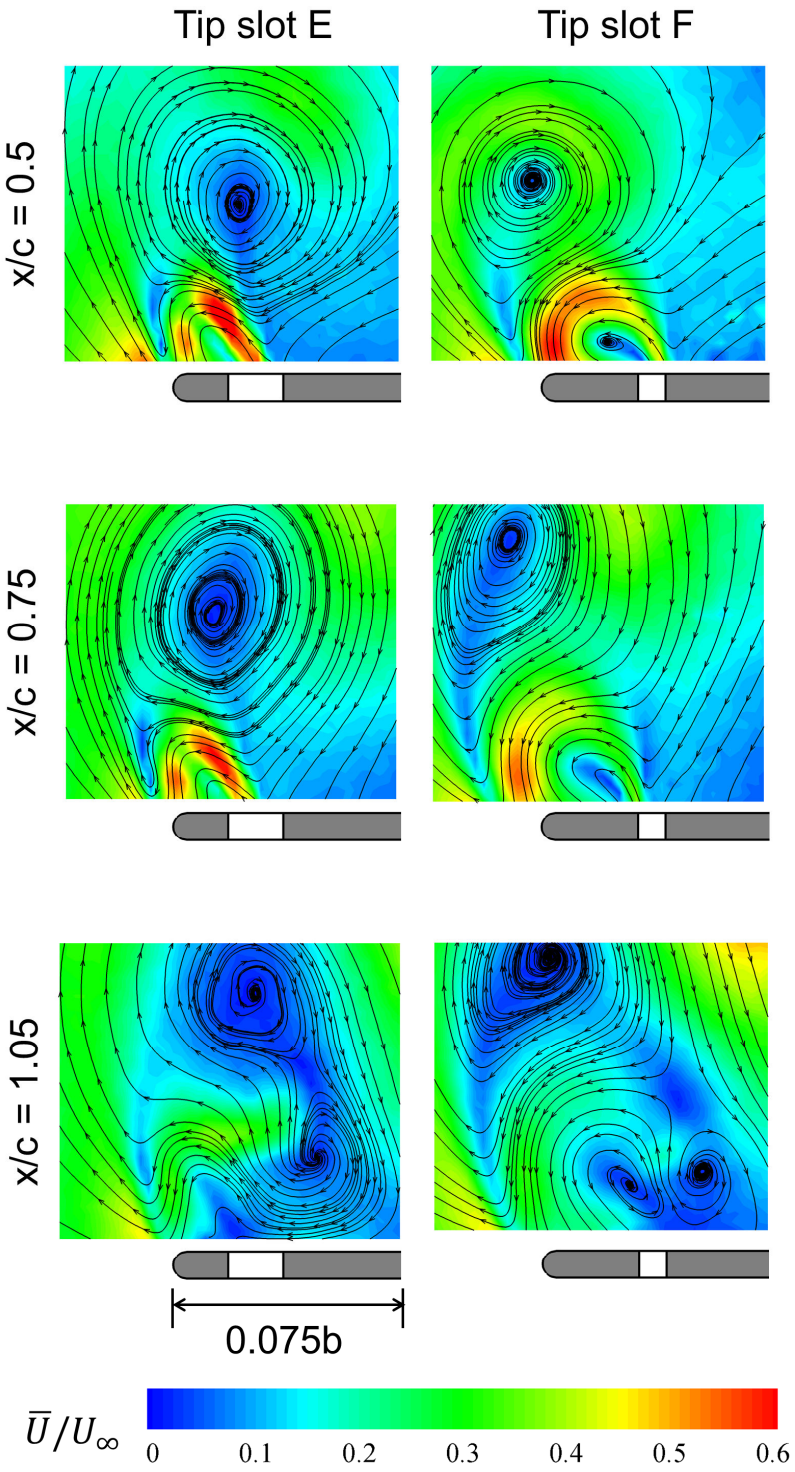


**Figure 11. Time-averaged velocity magnitude and streamline patterns over stationary flat plate wings with tip slot E and F at chordwise locations of $x/c$ = 0.5, 0.75 and 1.05 at $\alpha$ = 17° and $\Phi$ = 0°.**

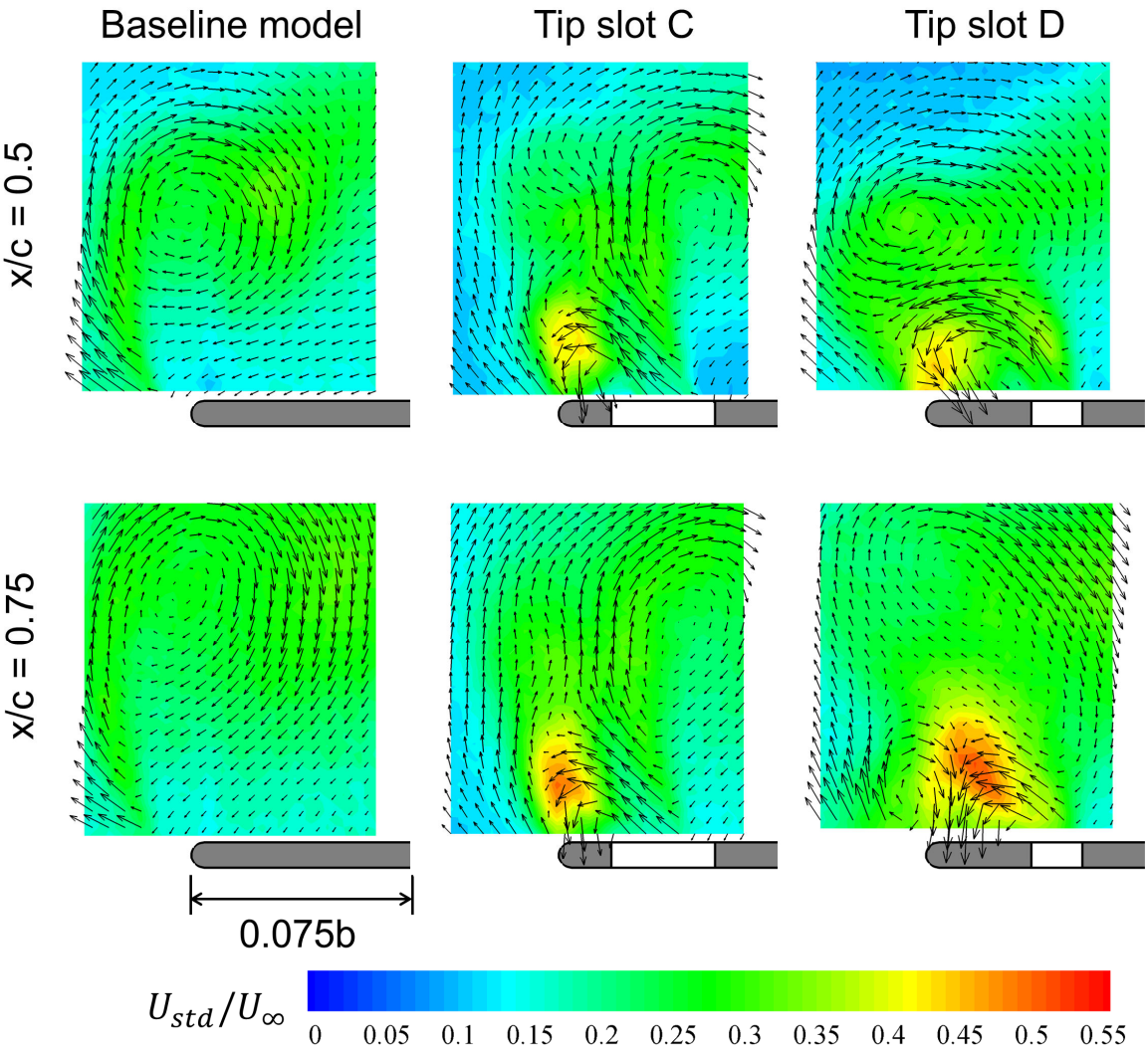


**Figure 12. Standard deviation of velocity fluctuations and time-averaged velocity vectors over the stationary baseline wing and flat plate wings with tip slot C and D at chordwise locations of *x/c* = 0.5 and 0.75, $\alpha = 17^o$ and $\Phi = 0^o$.**

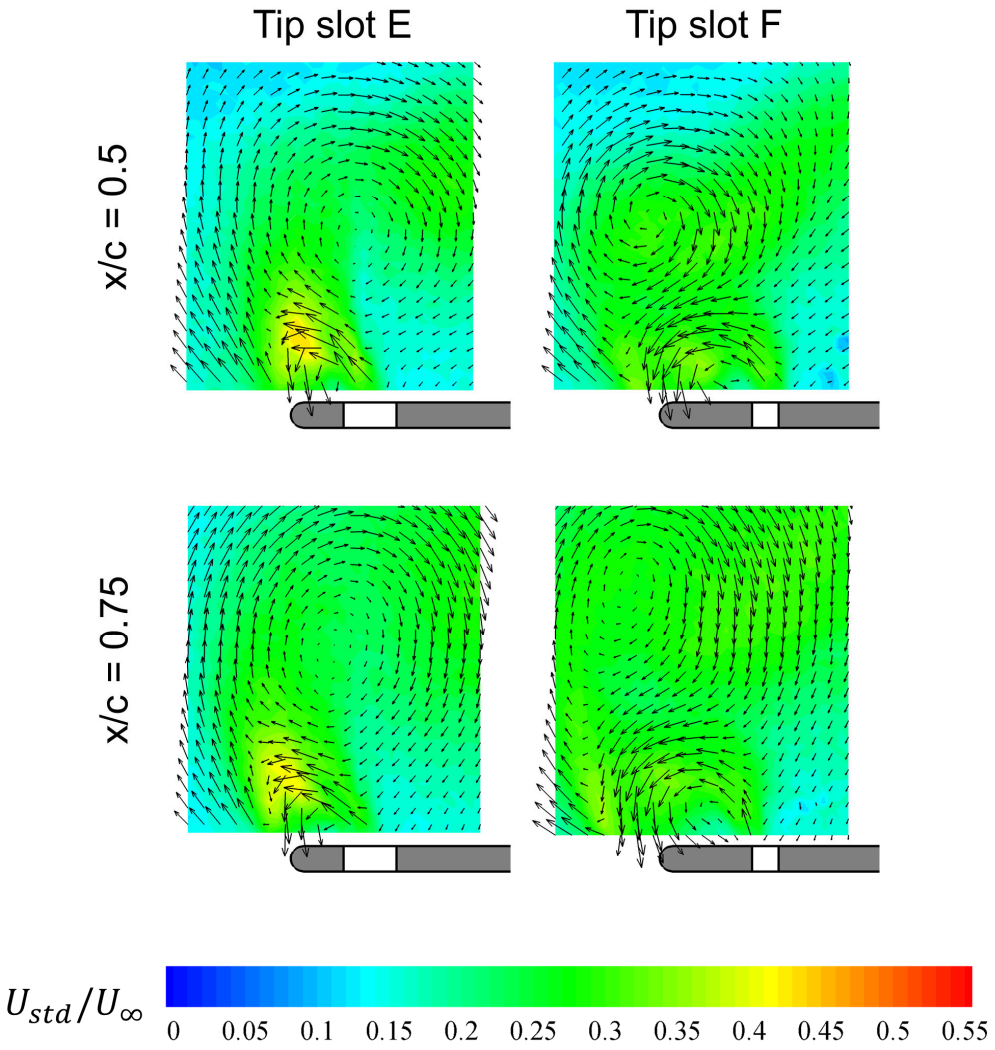


**Figure 13. Standard deviation of velocity fluctuations and time-averaged velocity vectors over stationary flat plate wings with tip slot E and F at chordwise locations of *x/c* = 0.5 and 0.75, $\alpha$ = 17° and $\Phi$ = 0°.**

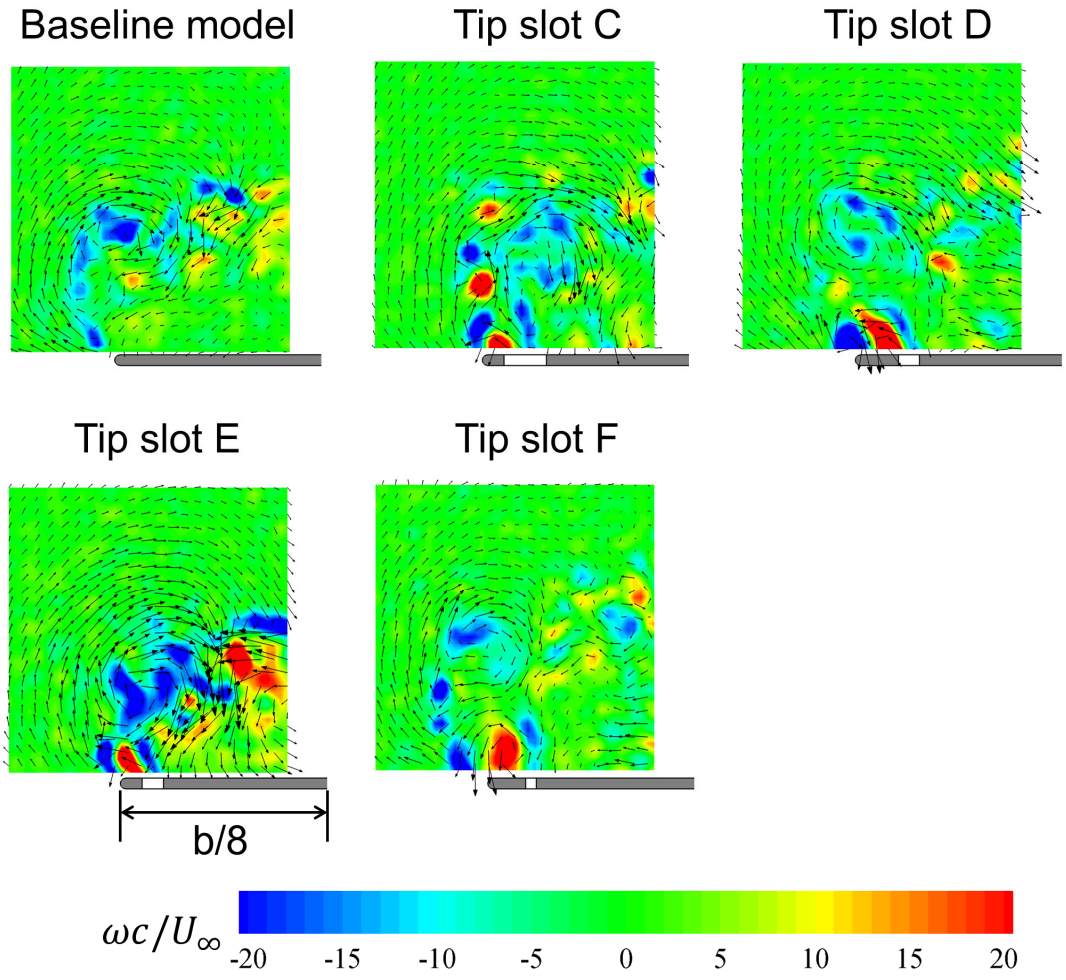


**Figure 14. Instantaneous vorticity patterns over the stationary baseline model and flat plate wings with tip slot C-F at chordwise location of $x/c$ = 0.75, $\alpha$ = 17° and $\Phi$ = 0°.**

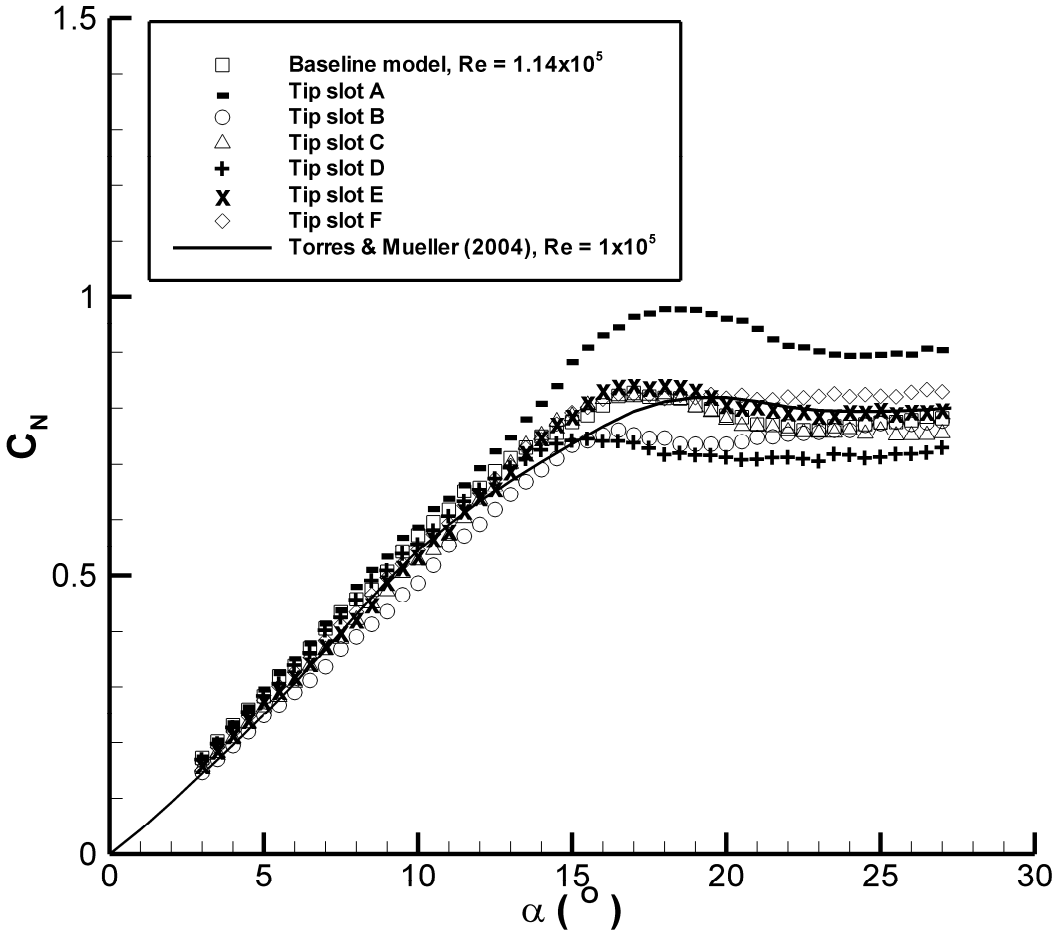


**Figure 15. Variation of normal force coefficient as a function of angle of attack for *AR* = 2 baseline wing and flat plate wings with tip slot A to F.**